UDC 551.576.11:551.574.14

Numerical Experiments on the Relation Between Microphysics and Dynamics in Cumulus Convection

F. W. MURRAY and L. R. KOENIG—*The Rand Corporation, Santa Monica, Calif.*

ABSTRACT—An existing numerical model of cumulus growth, treating condensation but not precipitation, is modified by the incorporation of a parameterized treatment of liquid phase microphysics. This modification improves the realism of the results in several important respects; among them are maximum height of cloud growth, maximum liquid content, amount and distribution of temperature departure, cloud shape, and occurrence and strength of subcloud downdraft. We found that one of the most important controlling features is the rate of evaporation of droplets. In particular, the introduction of a class of large particles with relatively slow evaporation rate produces a smaller temperature deficit at the cloud summit, hence more vigorous cloud growth. In this model, the upper and lower parts of he cloud are, to a large extent, decoupled dynamically, the development of a strong subcloud downdraft by evaporation of precipitation having little effect on the ultimate extent of cloud growth.

1. INTRODUCTION

The first generation of two-dimensional, numerical models of cumulus convection (Malkus and Witt 1959, Ogura 1962) described processes in dry air. This type of model shed some light on the circulations in convective systems but was unsatisfactory because latent heat is a major source of energy for cumulus clouds. The second generation (Ogura 1963) incorporated condensation and evaporation of water but treated the liquid phase as through it were another gas; that is, microphysical processes involving drops were ignored. Condensed liquid was assumed to move with the air and not to fall out. A considerable degree of realism was attained with this type of model, but there were some obvious shortcomings; among these are the lack of gravitational separation and a rainfall mechanism. Clearly, a more realistic treatment of cloud microphysics is desirable.

One criticism leveled against the model with no fallout of precipitation is that it tends to develop excessively large values of liquid water content, with consequent "loading" that decreases buoyancy and inhibits cloud growth. A model with fallout could determine the relative dynamic importance of water loading and other processes. But introduction of fallout requires some knowledge of drop-size distribution, which in turn involves a number of microphysical processes.

A variety of numerical models of cloud microphysics have been developed (e.g., Koenig 1966), but they cannot readily be combined with the dynamic models because of a gross mismatch of scale and requirement for very large computer capacity. Even so, 'Arnason et al. (1969) have proposed such a scheme; they have not yet, however, carried it through to completion.

A less ambitious approach to the combination of dynamics and microphysics has been tried, however, with a considerable degree of success. This approach involves the parameterization of microphysical processes in terms of bulk quantities; it was pioneered by Kessler (1967, 1969) in terms of a kinematic cloud model and applied to a dynamic cloud model by 'Arnason et al. (1968). Numerous other investigators have now adopted parts or all of Kessler's parameterization for use in their cloud models.

The basis for Kessler's parameterization is the conservation of total water substance through a series of continuity and conversion equations. The drop-size spectrum is drastically simplified by dividing the liquid into only two categories: droplets small enough to move with the air and drops large enough to fall relative to the air. These two categories may loosely, but conveniently, be designated suspended water (Kessler refers to this category as "cloud" water) and precipitating water. The precipitating water is assumed to have the drop-size distribution described by Marshall and Palmer (1948), but all drops are assumed to fall relative to the air with the terminal velocity appropriate to the volume-median drop size.

There are two processes by which suspended water can be converted to precipitating water. The first is autoconversion, which is a coalescence of small droplets; this depends on the bulk density of suspended water. The second is collection, which is a coalescence of large and small drops due to their differential velocity; this depends on the bulk densities of both suspended water and precipitating water. Kessler also parameterizes the evaporation of precipitating water when it enters a subsaturated region. Since this occurs at a finite rate, it is possible for liquid water to continue to exist even though the air is not saturated.

Portions of Kessler's parameterization have been used successfully in several one-dimensional cloud models (e.g., Simpson and Wiggert 1969, Weinstein 1970), and some of the effects of varying the parameters and equations have been discussed. The application to two dimensions poses some additional problems but it has been accomplished by

476-264 O - 72 - 3

TABLE 1.—*Symbols used in this paper*

$\mathbf{e}_\theta$	azimuthal unit vector
$\mathbf{k}$	vertical unit vector
$\mathbf{v}$	velocity of air parcel
$\boldsymbol{\omega}$	vorticity
B	buoyancy
D	mesh length
D_b	relative dispersion of drops
E	collection efficiency
L	latent heat of condensation
N_b	initial number concentration of drops
N_0	intercept of Marshall-Palmer curve
R	depth of rainfall
R_d	gas constant for dry air
S_1	rate of condensation
S_2	rate of autoconversion
S_3	rate of collection
S_4	rate of evaporation of precipitation
S_5	net rate of fallout of precipitation
T	temperature
$\overline{T}$	temperature at a given altitude at initial time
T'	departure of temperature from its value at initial time for the given altitude
T_v'	departure of virtual temperature from its value at initial time for the given altitude
T_{vm}	mean value of virtual temperature at initial time over the whole region
V	terminal velocity of water drops
V_0	terminal velocity of water drops at standard temperature and density
$a_1, \ldots, a_6$	parameters used to compute terminal velocity
c_p	specific heat of dry air at constant pressure
c_{pv}	specific heat of water vapor at constant pressure
c_w	specific heat of liquid water
g	acceleration due to gravity
p'	departure of air pressure from its value at initial time for the given altitude
q_v	mixing ratio of water vapor to dry air
q_s	saturation value of q_v
q_c	mixing ratio of suspended water to dry air
q_p	mixing ratio of precipitating water to dry air
r	radial coordinate; also drop radius
t	time
u	radial component of wind
w	vertical component of wind
z	vertical coordinate
δt	time step
ϵ	ratio of molecular weights of water vapor and dry air
η	azimuthal component of vorticity
θ	azimuthal coordinate
ν_M	eddy diffusion coefficient for momentum
ν_T	eddy diffusion coefficient for temperature
ν_v	eddy diffusion coefficient for water vapor
ν_c	eddy diffusion coefficient for cloud water
ν_p	eddy diffusion coefficient for precipitation water
ρ	air density
ρ_m	mean value of air density at initial time over the whole region
$\overline{\rho}_d$	density of dry air at a given altitude at initial time
$\phi_1, \ldots, \phi_9$	microphysics parameters; see table 2
ψ	stream function

'Arnason et al. (1968) and by Liu and Orville (1969) using a version of the parameterization proposed by Srivastava (1967). However, no specific study of the way the inclusion of parameterized microphysics affects a two-dimensional model has been published. It is the purpose of this paper to fill this gap and, by making use of the results obtained thereby, to infer something about the nature of the growth and decay of real cumulus clouds.

2. MATHEMATICAL DESCRIPTION OF THE MODEL

The basis for the model used in the present experiment is the two-dimensional nonprecipitating model described by Murray (1970). However, in accordance with Kessler's scheme for treating microphysical processes, the liquid water has been divided into suspended and precipitating water. The processes of evaporation and condensation treated by the old model now describe conversions between vapor and suspended water, and their rate is such that the air can never be subsaturated in the presence of suspended water or supersaturated. In addition, suspended water may be transformed to precipitating water by autoconversion and collection, and precipitating water falls relative to the air (but moves with the air horizontally) and evaporates at a slower rate than suspended water.

The Boussinesq approximation is used, so the equation of motion is

$$\frac{\partial \mathbf{v}}{\partial t}=-\mathbf{v}\cdot\nabla\mathbf{v}-\frac{1}{\rho_m}\nabla p'+g\left(\frac{T_v'}{T_{vm}}-q_c-q_p\right)\mathbf{k}+\nu_M\nabla^2\mathbf{v} \quad (1)$$

and the continuity equation is

$$\nabla\cdot\mathbf{v}=0. \quad (2)$$

The symbols used in this paper are defined in table 1.

Let

$$B=g\left(\frac{T_v'}{T_{vm}}-q_c-q_p\right). \quad (3)$$

This expresses the buoyancy force in terms of three variables:

1. The buoyancy depends on the departure of virtual temperature (i.e., of density of the moist air) from its basic state.
2. The buoyancy depends on the weight of the suspended water. Since this water moves with air, its weight represents a simple downward force on the parcel of which it is a part.
3. The buoyancy depends on the weight of the precipitating water. This water is moving downward relative to the air parcel at its terminal velocity, which by definition is that speed at which the aerodynamic drag is exactly balanced by the weight. Hence, the downward force of the relatively falling drops takes the same form as the downward force of the relatively stationary droplets.

If we substitute eq (3) into eq (1), take the curl, and make use of eq (2), we get the vorticity equation,

$$\frac{\partial \boldsymbol{\omega}}{\partial t}=\nabla\times(\mathbf{v}\times\boldsymbol{\omega})+\nabla\times B\mathbf{k}-\nu_M\nabla\times(\nabla\times\boldsymbol{\omega}), \quad (4)$$

where $\boldsymbol{\omega}=\nabla\times\mathbf{v}$. In cylindrical coordinates (r, θ, z), with the assumption of axial symmetry and no rotation, eq (4)

becomes

$$\frac{\partial \eta}{\partial t}=-\left[\frac{\partial}{\partial r}(u\eta)+\frac{\partial}{\partial z}(w\eta)\right]-\frac{\partial B}{\partial r}+\nu_M\left\{\frac{\partial}{\partial r}\left[\frac{1}{r}\frac{\partial}{\partial r}(r\eta)\right]+\frac{\partial^2\eta}{\partial z^2}\right\}. \tag{5}$$

Here, the horizontal and vertical components of wind are defined by a stream function, ψ, according to

$$u=-\frac{1}{r}\frac{\partial \psi}{\partial z} \quad \text{and} \quad w=\frac{1}{r}\frac{\partial \psi}{\partial r}, \tag{6}$$

and the tangential component of vorticity is

$$\eta=-\left(\frac{\partial w}{\partial r}-\frac{\partial u}{\partial z}\right)=-\frac{1}{r}\left[r\frac{\partial}{\partial r}\left(\frac{1}{r}\frac{\partial \psi}{\partial r}\right)+\frac{\partial^2\psi}{\partial z^2}\right]$$
$$=\mathbf{e}_\theta\cdot\nabla\times\mathbf{v}=\mathbf{e}_\theta\cdot\boldsymbol{\omega}. \tag{7}$$

Except for fallout and eddy diffusion, the total water is individually conserved. Hence,

$$\frac{dq_v}{dt}=-S_1+S_4+\nu_v\nabla^2 q_v, \tag{8}$$

$$\frac{dq_c}{dt}=S_1-S_2-S_3+\nu_c\nabla^2 q_c, \tag{9}$$

and

$$\frac{dq_p}{dt}=S_2+S_3-S_4-S_5+\nu_p\nabla^2 q_p \tag{10}$$

where S_1 is the rate of condensation, S_2 is the rate of autoconversion, S_3 is the rate of collection, S_4 is the rate of evaporation of precipitating water, and S_5 is the net rate of fallout. It has generally been found desirable to let $\nu_p=0$, but $\nu_v=\nu_c\neq 0$.

The thermodynamic equation is

$$\frac{dT'}{dt}=\frac{L(S_1-S_4)-gw}{c_p+q_v c_{pv}+(q_c+q_p)c_w}-\frac{d\overline{T}}{dt}+\nu_T\nabla^2 T'. \tag{11}$$

As in the nonprecipitating model of Murray (1970), the rate of condensation is

$$S_1=\frac{1-\dfrac{c_pT-Lq_s}{\epsilon L}}{L+\dfrac{c_pR_dT^2}{Lq_s(\epsilon+q_s)}}gw \qquad \text{if } q_v=q_s$$

and (12)

$$S_1=0 \qquad \text{if } q_v<q_s.$$

If $w<0$, then S_1 is the rate of evaporation of suspended water. In this case, the total evaporation during a time step may not exceed in magnitude the initial value of q_c for that time step. Care is taken that the condition $q_v>q_s$ never exists when eq (12) is to be solved.

TABLE 2.—*Values of microphysical parameters (SI units)*

$\phi_1=10^{-3}\,s^{-1}$
$\phi_2=0.5\times10^{-3}$ kg·m^{-3}
$\phi_3=6.96\times10^{-4}\,E\,N_0^{0.125}\times10^{2.625}$
$\phi_4=1.93\times10^{-6}\,N_0^{0.35}\times10^{1.95}$
$\phi_6=-38.3(1{,}000/N_0)^{0.125}$
$\phi_7=10/3$
$\phi_8=7.32\times10^{-6}\,N_b/D_b$
$\phi_9=4.35\times10^4(1{,}000/N_0)^{0.25}$
$N_0=10^7$ [intercept of Marshall-Palmer (1948) curve]
$N_b=\begin{cases}50 \text{ (maritime)}\\ 2{,}000 \text{ (continental)}\end{cases}$ [initial number concentration of drops]
$D_b=\begin{cases}0.366 \text{ (maritime)}\\ 0.146 \text{ (continental)}\end{cases}$ [relative dispersion of drops]
$E=1$ [collection efficiency]

The rate of autoconversion, according to Kessler, is

$$S_2=\phi_1\left(q_c-\frac{\phi_2}{\bar{\rho}_d}\right) \qquad \text{if } q_c>\frac{\phi_2}{\bar{\rho}_d}$$

and (13)

$$S_2=0 \qquad \text{if } q_c\leq\frac{\phi_2}{\bar{\rho}_d}.$$

(The recommended values of the parameters ϕ_i are given in table 2.) In this formulation, autoconversion does not occur unless q_c exceeds a certain threshold value. Berry (1968) has proposed an alternative formulation that does not have this property; it is

$$S_2=\frac{\phi_7\bar{\rho}_d q_c^2}{1+\dfrac{\phi_8}{\bar{\rho}_d q_c}}. \tag{14}$$

Berry's formulation for autoconversion is based on more accurate coalescence equations than Kessler's. Simpson and Wiggert (1969) have used it with two sets of parameters, one for clouds over land and one for clouds over water. All three formulations have been used in the present study.

The rate of collection is

$$S_3=\phi_3 q_c(\bar{\rho}_d q_p)^{0.875}. \tag{15}$$

The rate of evaporation of precipitating water is

$$S_4=\phi_4(q_s-q_v)(\bar{\rho}_d q_p)^{0.65} \qquad \text{if } q_v<q_s$$

and (16)

$$S_4=0 \qquad \text{if } q_v\geq q_s.$$

The net rate of fallout of precipitating water, S_5, cannot readily be expressed in the same Lagrangian manner as the other terms. It has been found expedient to solve eq (10) with S_5 omitted and then to correct the result for fallout; this is discussed at greater length in section 4. Whatever the method used to evaluate S_5, however, the terminal velocity of the volume-median water drop must be known. Kessler (1967) suggests the relation

$$V=\phi_6(\bar{\rho}_d q_p)^{0.125}. \tag{17}$$

Note that, by convention, $V \leq 0$. Kessler (1969) also suggests a correction for altitude, amounting to 24 percent at 600 mb, that could be incorporated into eq (17) After several computer runs were made using eq (17), we noted that when q_p is large eq (17) gives errors in excess of 10 percent with respect to the sea-level observations of Gunn and Kinzer (1949). At intermediate values, the error is smaller, but for very small values of q_p, the error can be several hundred percent. This had also been noted by Liu and Orville (1969). Of course, not much water is involved when q_p is small; however, it was deemed desirable to find a better expression for V than eq (17).

By a process of curve fitting, Wobus et al. (1971) matched the experimental values of Gunn and Kinzer to a high degree of accuracy. First, the drop radius (in μm) is determined. According to Kessler (1967, 1969) this is

$$r=\phi_9(\bar{\rho}_d q_p)^{0.25}. \tag{18}$$

From this, the terminal velocity (in m/s) at sea level is found as follows:

$$\begin{aligned}
V_0&=-1.197\times10^{-4}r^2 \\
&\quad +8.64\times10^{-11}r^5 \\
&\quad +1.44\times10^{-13}r^6 && \text{if } r\leq 50, \\
V_0&=-9\times10^{-3}r+0.18 && \text{if } 50<r\leq 230, \\
V_0&=-0.008r-0.07+a_1 && \text{if } 230<r\leq 450,
\end{aligned}$$

and (19)

$$V_0-\frac{5.545}{a_3}-9.215+a_1 \qquad \text{if } 450<r$$

where

$$a_1=\frac{0.4}{r-210},$$

$$a_2=r-450,$$

and

$$\begin{aligned}
a_3&=2.036791\times10^{-15}a_2^5-3.815343\times10^{-12}a_2^4 \\
&\quad +4.516634\times10^{-9}a_2^3-8.020389\times10^{-7}a_2^2 \\
&\quad +1.44274121\times10^{-3}a_2+1.
\end{aligned}$$

Finally, the terminal velocity appropriate to the actual density and viscosity of the air is found by means of

$$V=a_5-(a_5^2+a_6)^{1/2} \tag{20}$$

where

$$a_4=\frac{\rho}{V_0}\left(\frac{0.2177076r}{V_0}+\frac{1817.8}{r}\right),$$

$$a_5=\frac{6}{ra_4}\left(775.7257-\frac{719813.4}{T+918.768}\right),$$

and

$$a_6=\frac{0.261249r}{a_4}.$$

In all the runs described herein, eq (20) was used in preference to eq (17).

In the microphysical equations of this paper, mixing ratios are multiplied by $\bar{\rho}_d$. We must do this because the original parameterization was developed in terms of bulk density (mass of water per unit volume of dry air), whereas the hydrodynamic equations are in terms of mixing ratio (mass of water per unit mass of dry air). An extremely small error is incurred by using the initial density rather than the current density at the specified altitude.

3. BOUNDARY AND INITIAL CONDITIONS

The principal boundary conditions are the assumption of axial symmetry about the line $r=0$ and of rigid, free-slip boundaries at the outer, lower, and upper limits.

Initially, the air is assumed to be at rest and horizontally homogeneous and to contain no liquid water. In the present study, the basic sounding (San Juan, P.R., 2300 GMT, Aug. 20, 1963) and the initial impulse used to start the convection were identical to those in the previous study by Murray (1970).

The model space was a cylinder of 6-km radius and 9-km depth. Comparison with a run having a ceiling of 7 km showed no significant differences, indicating that except in run 6, which is not realistic in any case, there is no adverse interaction between the cloud and the upper boundary. The outer boundary is even more remote in a dynamical sense.

Special effort has been made to assure the conservation of total mass of water. In general, this is accomplished to within 0.2 percent for 60 min of simulated time ($\approx$450 time steps).

4. METHOD OF SOLUTION

Within any time step, the order of operations is as follows:

1. The vorticity equation, eq (5), is solved for η at the new time. An Eulerian scheme is used with centered differences in both space and time.

2. The value of ψ is found from η by relaxation using eq (7), and u and w are then calculated by means of eq (6).

3. For each gridpoint, an upstream point is found such that the air parcel at the upstream point at the beginning of the time step moves to the gridpoint at the end of the time step. The initial value of each variable (T', q_c, q_p, etc.) is found at the upstream point by bilinear interpolation. For the sake of internal consistency, some variables are not interpolated directly but are calculated from other interpolated variables.

4. If $q_v>q_s$ at the upstream point, enough suspended water is condensed instantaneously to bring the air to exact saturation. This alters the values of q_v, q_c, q_s, and T'. If $q_v<q_s$ and $q_c>0$, evaporation of suspended water occurs in the same manner, but does not exceed q_c. If, following the latter check and correction, $q_v<q_s$, step 5 is skipped.

5. Using current values of all variables, we determine S_1, S_2, and S_3. These values are used in conjunction with eq (8)–(11) to get intermediate new values for q_v, q_c, q_p, and T' under the assumption that $S_4=S_5=0$.

6. The eddy-diffusion terms of eq (8)–(11) and the terms $-gw/[c_p+q_pc_{pv}+(q_c+q_p)c_w]$ and $-d\bar{T}/dt$ of eq (11) are incorporated into the intermediate values.

7. Terminal velocity, V, is computed from eq (20), and the intermediate value of q_p, determined in step 5 for the gridpoint under the assumption that precipitating water moves with the air, is now assumed to apply to a point a distance of $|V\delta t|$ below the gridpoint. Under the assumption of linear variation of $\bar{\rho}_d q_p$ from one datum point to another, the new value of q_p at the gridpoint of height z_0 is found by solution of

$$q_p(z_0)=\frac{1}{D\bar{\rho}_d(z_0)}\int_{z_0-D/2}^{z_0+D/2}\bar{\rho}_d q_p dz \tag{21}$$

where D is the mesh length. If z_0 is the highest level for which $q_p(z_0+V\delta t)>0$, then it is assumed that $q_p(z_0+D/2)=0$; this suppresses the artificial upward migration of the cloudtop. At $z=0$, eq (21) is modified to

$$q_p(0)=\frac{2}{D\bar{\rho}_d(0)}\int_0^{D/2}\bar{\rho}_d q_p dz, \tag{22}$$

and the mass of water per unit horizontal area falling out as rain is

$$R=\int_{V(0)\delta t}^{0}\bar{\rho}_d q_p dz. \tag{23}$$

As it happens, this mass (in kg) is equal to the rain depth (in mm). (In this paper, the term "rain" refers to water that has fallen to the ground.) The procedure outlined above is almost exactly conservative of the sum of precipitating water and rainwater. The percent difference in the total mass of precipitating water and rainwater in a column before and after the computation is typically of the order of 10^{-14} percent.

8. The instantaneous correction of step 4 is again applied. This does not represent a physical process but a compensation for errors introduced by linear computation of nonlinear processes. The adjustment is slight.

9. If $q_v<q_s$ and $q_p>0$, S_4 is computed, and the values of q_v, q_p, and T' are appropriately adjusted through eq (8), (10), and (11).

5. SOME RESULTS OF THE RUNS

To determine the effects of several variations in the parameterization, we made six computer runs. All six had the same initial sounding and impulse [also used in the study by Murray (1970)], and, in all cases, the eddy-diffusion coefficients were $\nu_M=\nu_T=\nu_v=\nu_c=40$ m^2/s and $\nu_p=0$. The principal characteristics of the runs were as follows:

Run 1. The Kessler (1967, 1969) parameterization was used as described herein, except that the autoconversion threshold was made excessively high ($\phi_2=5\times10^4$ kg·m^{-3}). Consequently, no precipitating water could appear. This is essentially the same as the axisymmetric run described by Murray (1970), but small variations in the programs make them not quite identical.

Run 2. The Kessler parameterization was used without modification. The autoconversion threshold was normal ($\phi_2=0.5\times10^{-3}$ kg·m^{-3}).

Run 3. This run was identical to run 2 except that Berry's expression for autoconversion, eq (14), was used in place of Kessler's, eq (13). The parameters entering into ϕ_8 were those appropriate for clouds in a maritime air mass (table 2).

Run 4. This run was identical to run 3 except that the parameters entering into ϕ_8 were those appropriate for clouds in a continental air mass.

Run 5. This run was identical to run 3 except that eq (16) was modified to permit total evaporation of q_p within one time step provided that it did not make $q_s>q_s$.

Run 6. This run was identical to run 3 except that, in any process involving evaporation, the latent heat was set equal to zero. In any process involving condensation, latent heat had its usual value.

Comparison of run 1 with the others shows the effects of the change from a second-generation model (with condensation but no accounting for drop size) to a third-generation model (accounting for drop size in a simplified manner). Comparisons of runs 2–4 show, among other things, the effects of varying the rate at which large drops are produced, especially in the early stages. Runs 5 and 6 were added to test a hypothesis concerning evaporation that was suggested by the other runs.

A summary of some results of the six runs is given in table 3. All tabulated values except cloud efficiency and dissipation time refer to the central axis. Rainfall rates and amounts are area-weighted means for the axis and the first gridpoint away from it. Not surprisingly, the extreme values of the several variables are almost always found on the central axis. One notable exception is the negative temperature departure near the cloud summit, which occasionally reaches its greatest magnitude a grid unit or two away from the axis and a little below the level of the summit on the axis. This, perhaps, is merely an apparent feature, resulting from the inability of the finite-difference mesh to resolve the small-scale patterns of temperature departure (figs. 10–13).

Perusal of table 3 shows that in several respects the three runs with normal precipitation development (runs 2–4) are similar, but collectively they differ markedly from run 1, which has no precipitation. Among these properties are maximum cloud height (which is 1400–1800 m greater with precipitation than without it), extreme downdraft at 200 m (which is negligible without precipitation, but considerable with it), summit temperature departure (which is somewhat greater without precipitation than with it), and time of dissipation (which is considerably earlier without precipitation than with it). On the other hand, some properties, such as maximum liquid water content and maximum updraft strength, show no such clear-cut distinction. For the most part, the properties of runs 2–4 agree reasonably well with observations of natural clouds over the Caribbean Sea on the day in question (Simpson et al. 1965).

Partition of Total Water

The differences in maximum cloudtop height, as well as some other indices, suggest that some phenomenon associated with the inclusion of a fallout mechanism for liquid water results in more vigorous cloud growth. This is further borne out by figures 1–4, which show the variation with time of the total mass of water in each category (except vapor) of the computational domain. Two supplementary curves in these figures are for total airborne liquid water (the sum of suspended and precipitating

TABLE 3.—*Summary of cloud characteristics*

Run number	1	2	3	4	5	6
Description	No precipitation	Unmodified Kessler	Kessler with Berry autoconversion (maritime)	Kessler with Berry autoconversion (continental)	Kessler-Berry (maritime) with instantaneous evaporation of precipitation	Kessler-Berry (maritime) with no cooling due to evaporation
Maximum cloudtop						
Height (m)	4000	5600	5800	5400	4000	†8800
Time (min)	32	36	37	35	33	26
Maximum liquid water						
Amount (g/kg)	4. 73	4. 90	5. 02	4. 69	4. 37	16. 20
Height (m)	3800	2900	3000	3000	2800	6800
Time (min)	32	31	31	31	31	32
Maximum updraft						
Strength (m/s)	15. 34	13. 93	15. 07	14. 42	12. 65	20. 34
Height (m)	3400	3600	3600	3400	3200	8400
Time (min)	30	30	30	30	29	31
Extreme downdraft at 200 m						
Strength (m/s)	−0. 092	−4. 95	−5. 03	−5. 10	−11. 01	−2. 19
Time (min)	16	37	37	37	38	29
Time to reach −0.1 m/s (min)	—	20	15	28	16	16
Rainfall at axis						
Maximum rate* (mm/min)	—	0. 500	0. 525	0. 481	0. 268	‡2. 425
Time (min)	—	36	36	37	34	40
Total* (mm)	—	6. 4	7. 7	4. 8	2. 2	‡30. 0
Time first reaches ground (min)	—	19	16	24	29	15
Maximum cloud efficiency (%)	—	68	82	50	25	‡17
Summit temperature departure						
Extreme (°C)	−2. 77	−1. 38	−1. 72	−1. 60	−2. 24	−1. 07
Time (min)	31	26	29	35	32	23
Cloud dissipation						
Time (min)	53	75	76	74	43	>40

*Integrated over a disk 300 m in radius
†Cloud reached top of computational space.
‡Computation was terminated at 40 min.

water) and total liquid (the sum of total airborne and fallen rain). In figure 1, of course, the curves of suspended water and total liquid are identical. Figures 2–4 all show substantially more liquid than figure 1, confirming the impression of greater activity. Paradoxically, however, the curves of cumulative condensation, or total mass of water condensed up to a given time, are almost identical in all four figures. This would suggest that it is not merely the innovation of allowing some of the condensed water to fall relative to the air that affects the dynamics of the cloud.

It has been proposed that the nonprecipitating model, by requiring the condensate to be carried with the air, contains an extra loading factor that decreases the buoyancy and damps the cloud development. This mechanism is probably at work, even though table 3 shows higher liquid water content for runs 2 and 3 than for run 1. It will be noted that the maximum of liquid water content occurs near the top of the cloud in run 1, well above the level of maximum updraft, but in runs 2–4 it occurs much lower, despite a much higher cloudtop. (Note also figs. 6 and 7.) It is, in fact, well below the level of maximum updraft, which is about the same in all four runs.

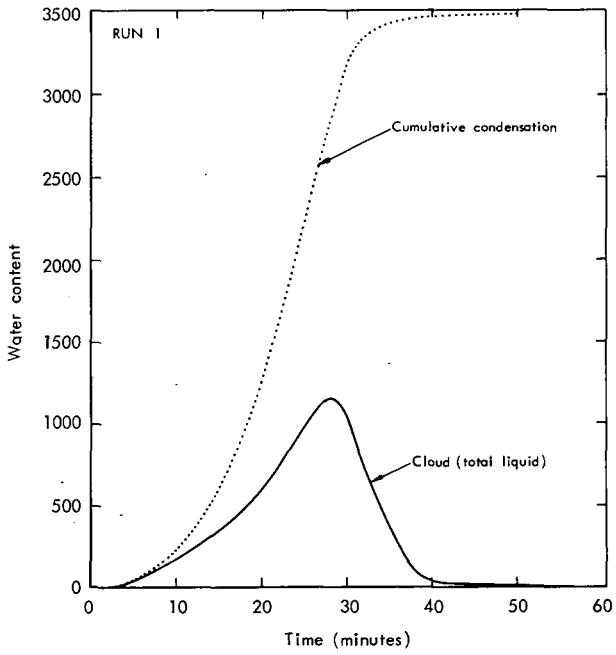

FIGURE 1.—Total liquid water (10^3 kg) and cumulative amount of water condensed versus time for run 1. (All liquid water is in the form of suspended droplets.)

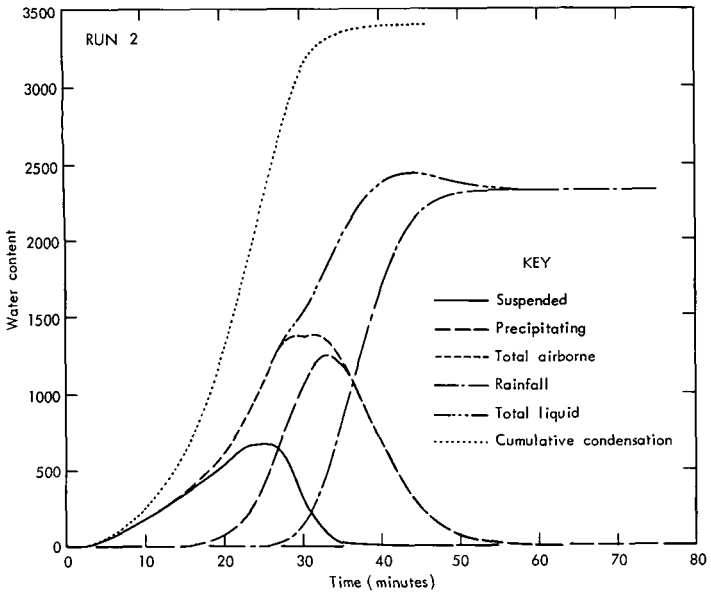

FIGURE 2.—Total liquid water (10^3 kg) in each form and cumulative amount of water condensed versus time for run 2.

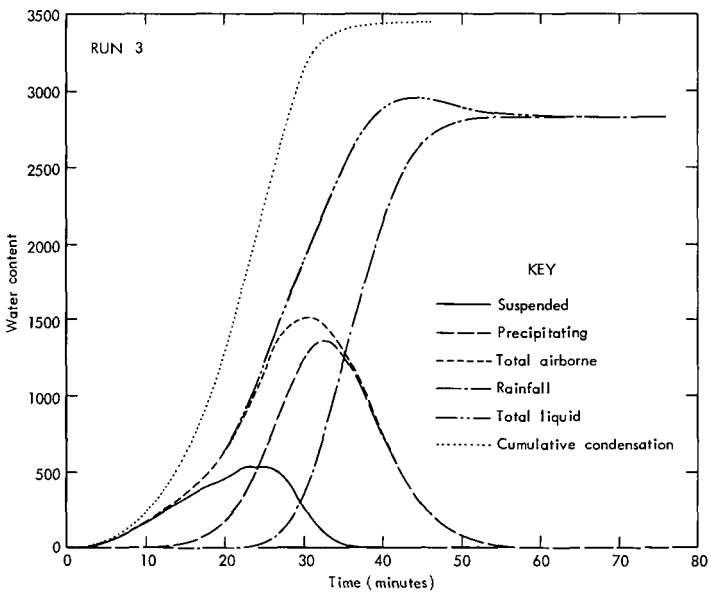

FIGURE 3.—Same as figure 2 for run 3.

Computed soundings for the central axis at 30 min of cloud time, when plotted on a thermodynamic diagram, show that the nonprecipitating model develops a profile of total water content that, except for a small decrease with height apparently due to diffusion, is nearly adiabatic. On the other hand, the profiles in the precipitating models show values of total water greater than adiabatic in the lower levels and less than adiabatic in the upper levels. Thus, as expected, the nonprecipitating model has its heaviest water loading near the top, where it evidently is most effective in damping cloud tower development. On the other hand, the precipitating models have it in lower levels relative to the top, where it has less effect on the maximum cloudtop height achieved.

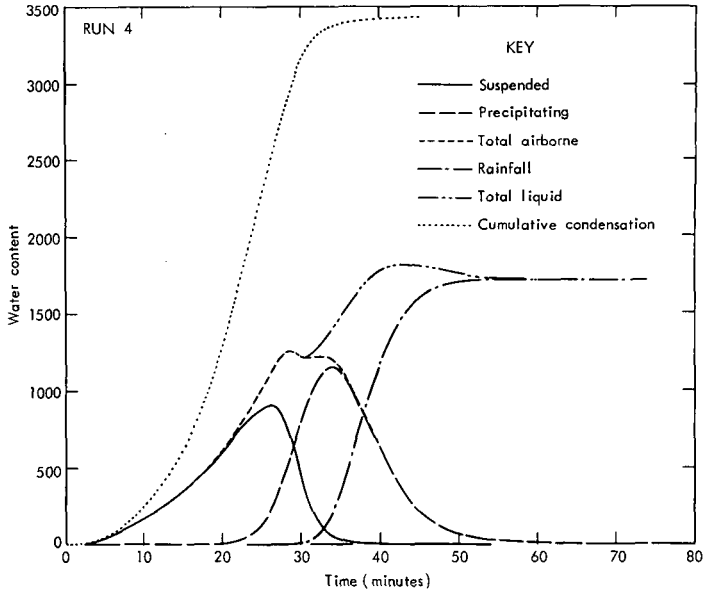

FIGURE 4.—Same as figure 2 for run 4.

Evaporation

Although loading is important, the computational results indicate that there is a much more powerful mechanism at work to differentiate between run 1 and runs 2–4. This mechanism is evaporation. In all four models, suspended water is assumed to consist of droplets so small that they can evaporate virtually instantaneously, and, therefore, they cannot persist from one time step to the next where the air is subsaturated. On the other hand, precipitating water consists of larger drops having finite evaporation rates. Accordingly, these drops do not necessarily completely evaporate in one time step, even though the air remains subsaturated. Consequently, the cooling associated with evaporation proceeds more slowly. The importance of the rate of evaporation is emphasized by runs 5 and 6, which are both basically like run 3 but have certain artificial conditions imposed on them. Run 5 illustrates rapid evaporation by allowing precipitating water in a subsaturated volume to evaporate instantaneously, as does suspended water. Thus, the dynamics of the cloud are influenced more rapidly by the thermal effects of evaporation in a subsaturated volume, but gravitational effects are unchanged. Run 6 illustrates the opposite extreme: both condensation and evaporation proceed as in run 3, but the latent heat of evaporation is taken to be zero. Thus, the dynamical consequences of evaporative cooling (but not of condensational warming or of water loading) are suppressed. The results are highly unrealistic, but, when taken together with the results of the other runs, they illuminate some of the important dynamical processes.

Because precipitating water was allowed to fall, the maximum of liquid water content in run 5 (instantaneous evaporation) occurred at the same low level as in runs 2–4, but its value was less. The maximum height of the cloudtop, however, was the same as in the nonprecipitating

model and much lower than in the other precipitating models. There are at least two consequences of the method of treating evaporation that contribute to this effect.

The first has to do with diffusion of liquid water. This can be of two types: explicit, through the eddy-diffusion terms, or implicit, through the finite-difference numerical procedures. In either case, the result is the same—at the cloudtop, liquid is diffused upward into a subsaturated environment. In runs 1 and 5, such water evaporated immediately and did not result in upward displacement of the cloud summit. In runs 2–4, however, some of the precipitating particles diffused upward from the cloudtop (by the implicit process, the explicit process having been disabled by specification of a zero coefficient of eddy diffusion for these particles) could continue to exist in a subsaturated environment. These subsaturated air volumes, formed by mixing cloudy air and ambient air, might contain sufficient water in the form of precipitating drops to be described as cloudy air, thereby increasing the height of the cloud summit. These processes are also in operation around the periphery of the cloud, with the result that instantaneous evaporation promotes erosion and dissipation of clouds, but introduction of a finite evaporation rate decreases the rate of erosion due to entrainment.

The second, and we believe more important, consequence of the method of treating evaporation has to do with evaporative cooling. In particular, the temperature departure from the ambient value near the cloudtop is markedly influenced by the amount of local evaporation. This, in turn, markedly influences the buoyancy. Because of the greater rate of evaporation, air near the top of a nonprecipitating or instantly evaporating cloud becomes colder and more dense than that associated with a normal precipitating cloud. This is borne out by the summit temperature departures shown in table 3.

By contrast, the temperature deficit near the summit in run 6 (zero heat of evaporation) was considerably smaller than that in the other runs. (The extreme value shown in table 3 is atypical; most of the time the deficit was even smaller.) The cloud responded by growing excessively, soon reaching the top of the computational space despite water loading three times as great as in the other runs. This is clear evidence that evaporational cooling has more dynamic effect than water loading.

Subcloud Downdraft

Effects near the summit, however, cannot account for all of the significant differences among the runs; hence, there are other important consequences of the method of treating evaporation. Most notable is the total amount of water condensed. As has been mentioned, this was almost identical for runs 1–4, but, as shown in figure 5, it was much smaller for run 5 (instantaneous evaporation). Also, the maximum updraft was smallest for run 5, but largest for run 1 (disregarding run 6). Apparently, a precipitating cloud with instant evaporation is in some important way different in its dynamics from a normal precipitating cloud or a nonprecipitating cloud. An explanation is suggested by

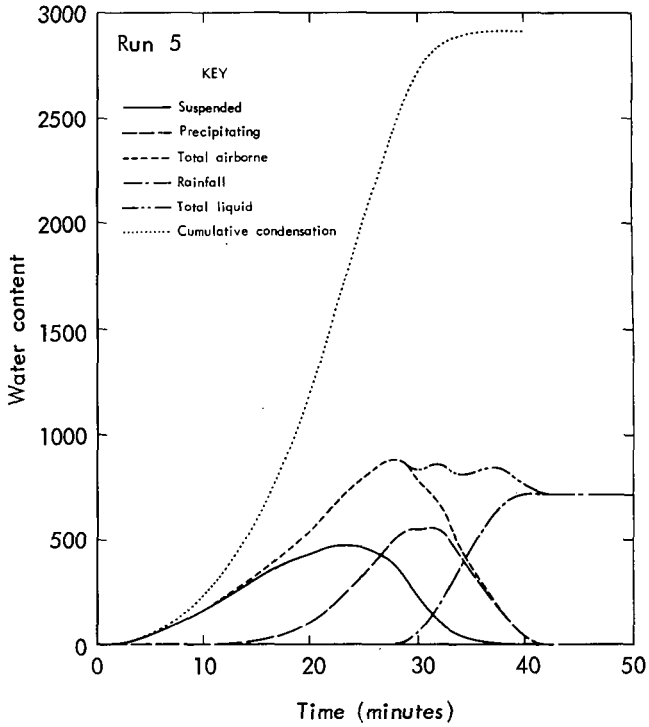

FIGURE 5.—Same as figure 2 for run 5.

the downdraft below the cloud. In run 1, liquid water could not fall below the cloud base, evaporate, and, by cooling the air, initiate a strong downdraft. By contrast, in runs 2–4, evaporation of falling precipitation led to a downdraft of about 5 m/s. The more rapid evaporation of run 5 led to a downdraft of 11 m/s. One might argue that the strong downdraft of run 5 cut the cloud off from its main source of moisture, inhibited its growth, and led to its early dissipation, but this argument is not valid, as comparison of runs 2–4 with run 1 will show. In this comparison, run 1, with the weakest downdraft, also had the least vertical development. On the other hand, the downdraft must have some inhibiting effect on cloud growth, for run 5, with its strong downdraft below cloud base, condensed less water and dissipated earlier than run 1, with negligible downdraft. Interestingly, run 6 developed a moderate downdraft below the cloud. Since evaporative cooling was not operative, water loading might be the cause. It should be noted, however, that the downdraft was less than half that of the normal cases despite much greater rainfall, and toward the end of the computation, when rainfall rate was at its peak, there was actually an updraft at low levels. Examination of streamlines suggests that in the later stages of run 6 the vigorous circulations were strongly affected by the boundaries, and the downdrafts and updrafts below the cloud were more closely related to the continuity condition than to the water loading.

Growth and Decay

The growth and decay of the cloud in runs 1, 3, and 5 are shown in figures 6, 7, and 8. Runs 2 and 4 so resemble run 3 that they have been omitted. On the other hand,

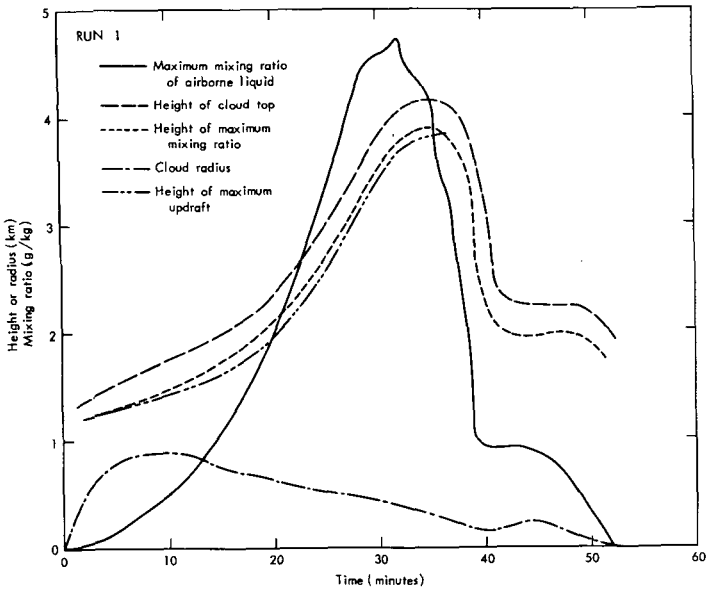

FIGURE 6.—Value of maximum mixing ratio of airborne liquid, height of maximum mixing ratio, height of maximum updraft, height of cloudtop, and radius of cloud versus time for run 1.

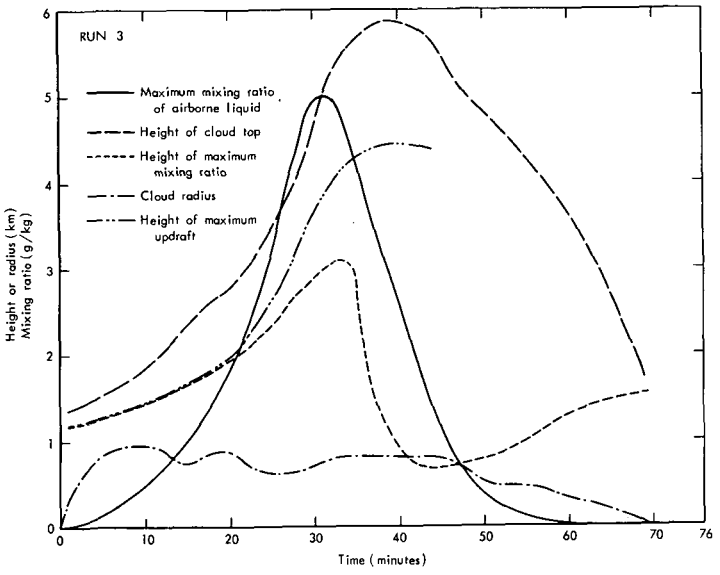

FIGURE 7.—Same as figure 6 for run 3.

whereas runs 1 and 5 resemble one another in some respects and differ in others, both are sharply differentiated from runs 2–4.

In all runs, the value of maximum mixing ratio of liquid increased at substantially the same rate, reaching similar peaks, although that of run 5 was somewhat smaller than the others. In runs 2–4, the magnitude then dropped off at a rate comparable to the previous rise, but in runs 1 and 5 the dropoff was precipitous. Run 1 showed a leveling of maximum mixing ratio after 40 min, followed by a drop to zero by 53 min. The cloudtop reached its maximum height a few minutes after the maximum value of mixing ratio, much higher in runs 2–4 than in runs 1 and 5. The descent of the cloudtop was at a moderate rate in runs 2–4 but dramatically rapid in runs 1 and 5. This behavior again suggests that in a dynamical context, rapid, unrealistic evaporation is equivalent to increasing the rate of entrainment.

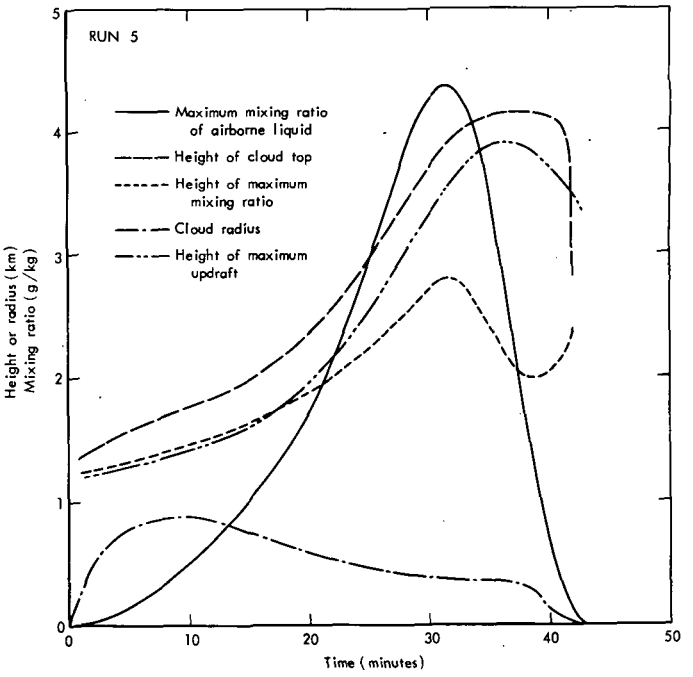

FIGURE 8.—Same as figure 6 for run 5.

The effect of the fallout of large drops is well illustrated by the height at which maximum mixing ratio occurred. In run 1, in which no fallout occurred, maximum mixing ratio was consistently just below the cloudtop and near the level of maximum updraft; in the others, it rose at a rate less rapid than that of the cloudtop, or even of the maximum updraft; and then started to fall before the cloudtop reached its peak. In runs 2–4, it fell to the lower part of the cloud and then rose as the cloud became depleted and decayed. In run 5, the behavior was the same, but the amount of descent was much less. From figure 7 one might conclude that the reduction in loading resulting from the fallout led to the increase in cloudtop height, but comparison of figures 6 and 8 shows this not to be the case. Instead, the cooling by evaporation near the summit and on the periphery seems to be the most important process in limiting cloud height.

In the present experiments, two clouds had very limited growth, the three that incorporated realistic microphysics reached moderate heights, and one grew uncontrollably. All six reached a radius of about 800 m within 5 or 6 min; this radius appears to be related to the size and shape of the initial impulse. Thereafter, the three categories behaved quite differently. The three runs with realistic microphysics kept nearly constant radius until the final stages of the life cycle (fig. 7). The two runs with rapid evaporation showed a steady decrease of radius after the first 10 min or so (figs. 6, 8). Run 6, with normal evaporation rate but no evaporative cooling, showed a rapid increase in radius after about 15 min, especially near the top of the cloud. These results support the views widely held among cloud modelers that height and radius are positively correlated and that the correlation comes about as a result of

476-264 O - 72 - 4

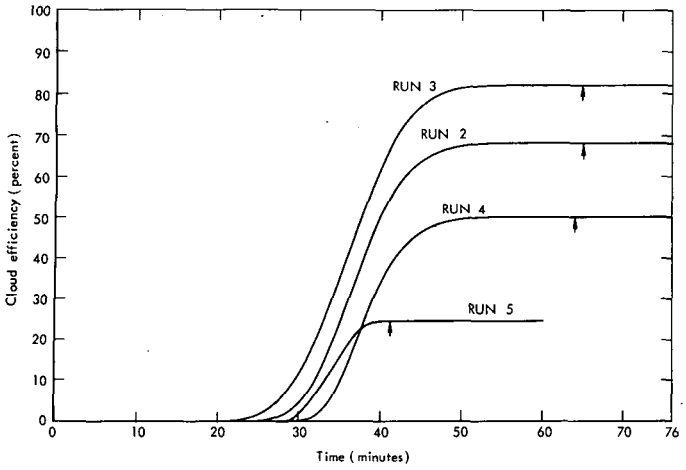

FIGURE 9.—Cloud efficiency versus time. Vertical arrows indicate time of cessation of rainfall at the ground.

greater relative entrainment of ambient air into narrower clouds than into wider ones.

Entrainment, as it is usually conceived, reduces the activity of cloud growth in several ways: one is the expenditure of energy in accelerating the entrained air (drag), and another is the decrease in buoyancy due to cooling resulting from the evaporation of cloud into the unsaturated entrained air. The former has been cited as an important term; however, the present results strongly suggest that evaporative cooling and consequent loss of buoyancy is dominant. This confirms the observation of Malkus (1954). Certainly in run 6, more air is being entrained into the cloud than in any of the other simulations, yet growth is unchecked. This can be the consequence only of elimination of the thermal effects of evaporation, for that is the only way in which runs 5 and 6 differ. Runs 1 and 5, in which evaporation is rapid and its effects are quickly felt, demonstrate rapid erosion of the cloud.

Cloud Efficiency

Since the total amount of water that has been condensed up to a given time is known, it is possible to compute cloud efficiency as the ratio of the amount of rain to the amount of condensation. Efficiency can alternatively be defined as the ratio of the amount of rain to the amount of water vapor rising through the cloudbase. This definition would lead to values about half as great as those we report. Table 3 shows that even though runs 2–4 are closely similar in many respects, they differ greatly in cloud efficiency; this is directly related to the amount of rain, since the amount of condensation is essentially the same. Run 5, however, has a significantly smaller amount of condensation, but, because it has so much less rain than the other three, its cloud efficiency is far lower.

The growth of efficiency with time is shown in figure 9. The differences among runs 2, 3, and 4 can be ascribed mainly to the rate at which suspended water is converted to precipitating water; that is, the "autoconversion" rate. The models that encourage early conversion have less evaporation, hence, earlier and more copious rain, and hence, higher cloud efficiency. Run 5 departs from this pattern, however, mainly because of the rapid evaporation below cloud base. When rain finally reached the ground, its initial rate of rainfall was high, so the cloud efficiency became temporarily greater than that of run 4. But soon, evaporation again took its toll, and even though the accumulated condensation was less than in the other cases, total rain was so diminished that the efficiency was very low. The vertical arrows in figure 9 show when rainfall ceased; it was very early in run 5.

Thermal Structure

The thermal structure of the clouds is illustrated in figures 10–12, which show cross-sections of virtual temperature for three cases about 10 min before, at, and 10 min after the time of maximum updraft, and in figure 13, which shows the cross-section for run 6 at 20 min (11 min before maximum updraft). The areas with more than 0.001 g of total airborne liquid water per kilogram of dry air are shaded. This is a more significant criterion than the area of 100-percent relative humidity, which merely shows that portion of the cloud in which active condensation is currently taking place. It should be noted that virtual temperature is always higher than actual temperature (by about 1°C for each 6 g/kg of mixing ratio of water vapor in the present instance); therefore, the figures show more extensive areas of warm air than they would if actual temperature had been plotted. Virtual temperature is used here because of its direct relation with buoyancy

The cold cap previously discussed with relation to the nonprecipitating cloud (Murray 1970) is quite apparent in figures 10 and 11. Two mechanisms have been proposed to explain its existence, and it is likely that both are operative. The first is the forced lifting and consequent dry-adiabatic cooling of subsaturated air at the cloud summit; only this effect is permitted in run 6. The second, and evidently more important, is evaporation. It will be noted in figures 10 and 11 that, for the two runs with instantaneous evaporation, the cold cap is outside the cloud, but with evaporation at a finite rate the cold cap is within the cloud. In figure 13, the cold cap is very weak despite rapid forced lifting near the cloud summit.

The effects of evaporation at the base of the cloud and at lower levels in the runs with fallout are clearly evident in the figures, as is the erosion that causes the clouds in runs 1 and 5 to contract laterally. On the basis of the present experiments, it would appear that this lateral erosion and cooling is the most important mechanism operating to cause the dissipation of the cloud. When this erosion is strong, as in the rapid-evaporation cases, the inflow of moist air in the lower part of the cloud is effectively cut off.

At the peak of development, the warm core, even for run 3, was very narrow. If actual rather than virtual temperature departures had been plotted, the positive

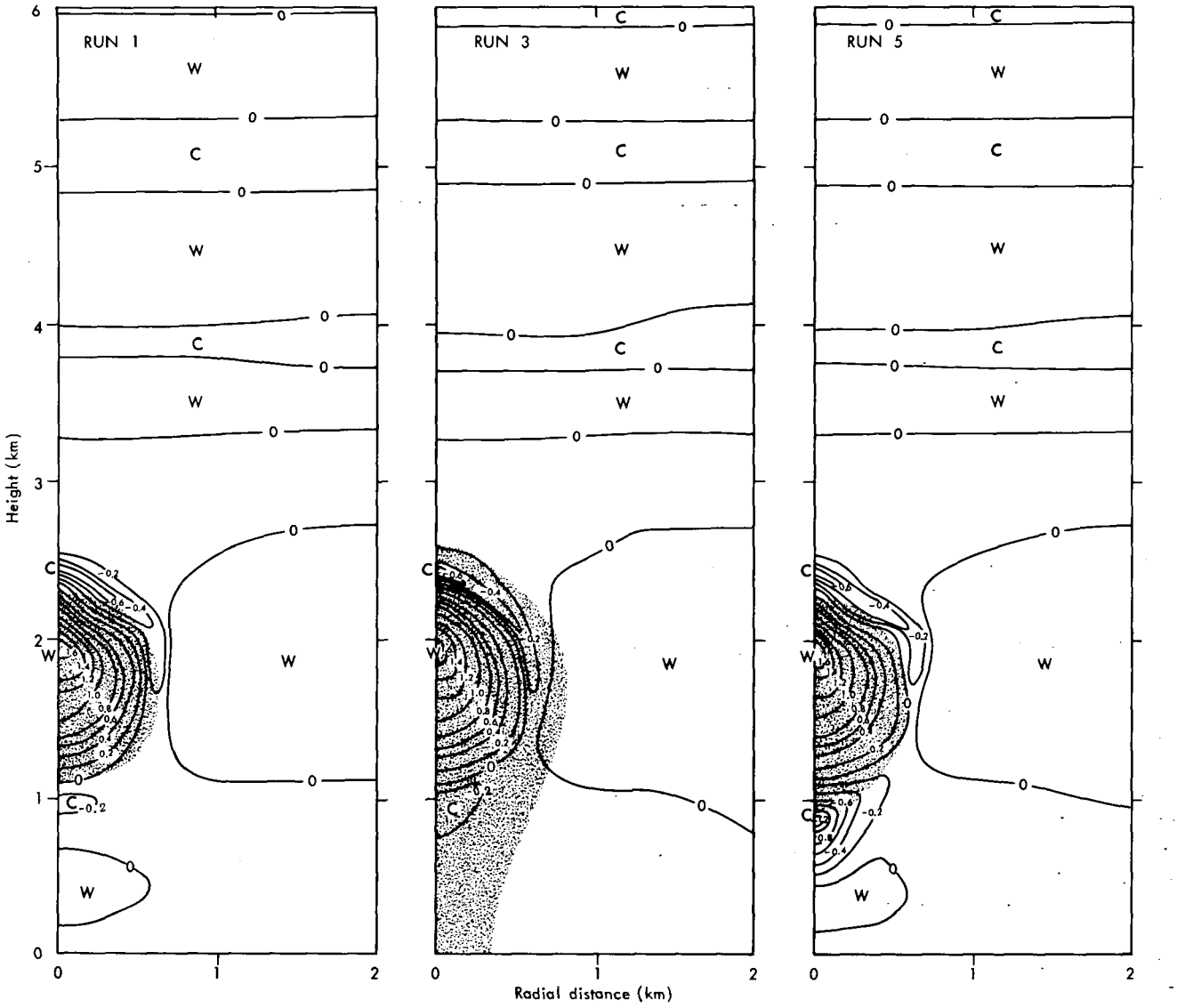

FIGURE 10.—Spatial distribution of departure of virtual temperature (°C) from its initial value for runs 1, 3, and 5 at 20 min. Area with more than 0.001 g/kg airborne liquid is shaded.

departures in the cloud would have been considerably smaller, and in some instances would even have gone negative. An aircraft probing a real cloud of this nature would be in the warm core only for a short time and might even miss it altogether. This finding is in agreement with actual reports of aircraft observations (Wexler and Malkus 1958) and of model results of Orville and Sloan (1970). In the period of decay, illustrated by figure 12, the warm core is still more elusive.

Autoconversion

The process of autoconversion postulated by Kessler (1967, 1969) is meant to parameterize the coalescence of small droplets to form large drops. Kessler took this to be linearly dependent on the suspended water content, with a threshold below which autoconversion does not occur [eq (13)]. Run 2 used this conversion with Kessler's recommended threshold. Berry (1968), by a theoretical argument, produced a formulation for autoconversion that depends on the cube of suspended water content [eq (14)]. Berry's formulation contains as parameters the initial number concentration of droplets and their relative dispersion. Using observations from South Florida and the Caribbean, Simpson and Wiggert (1969) proposed two sets of values for these parameters, one for clouds over water and one for clouds over land. These they designated "maritime" and "continental," respectively. In the present study, run 3 made use of the Berry autoconversion with the maritime parameters of Simpson and Wiggert, and run 4 made use of the Berry autoconversion with their continental parameters. In a later paper, Simpson and Wiggert (1971) used a considerably smaller value of number concentration (500 as compared with 2,000), which they call the "Florida conversion." Use of this smaller number would have sped up the rate of auto-

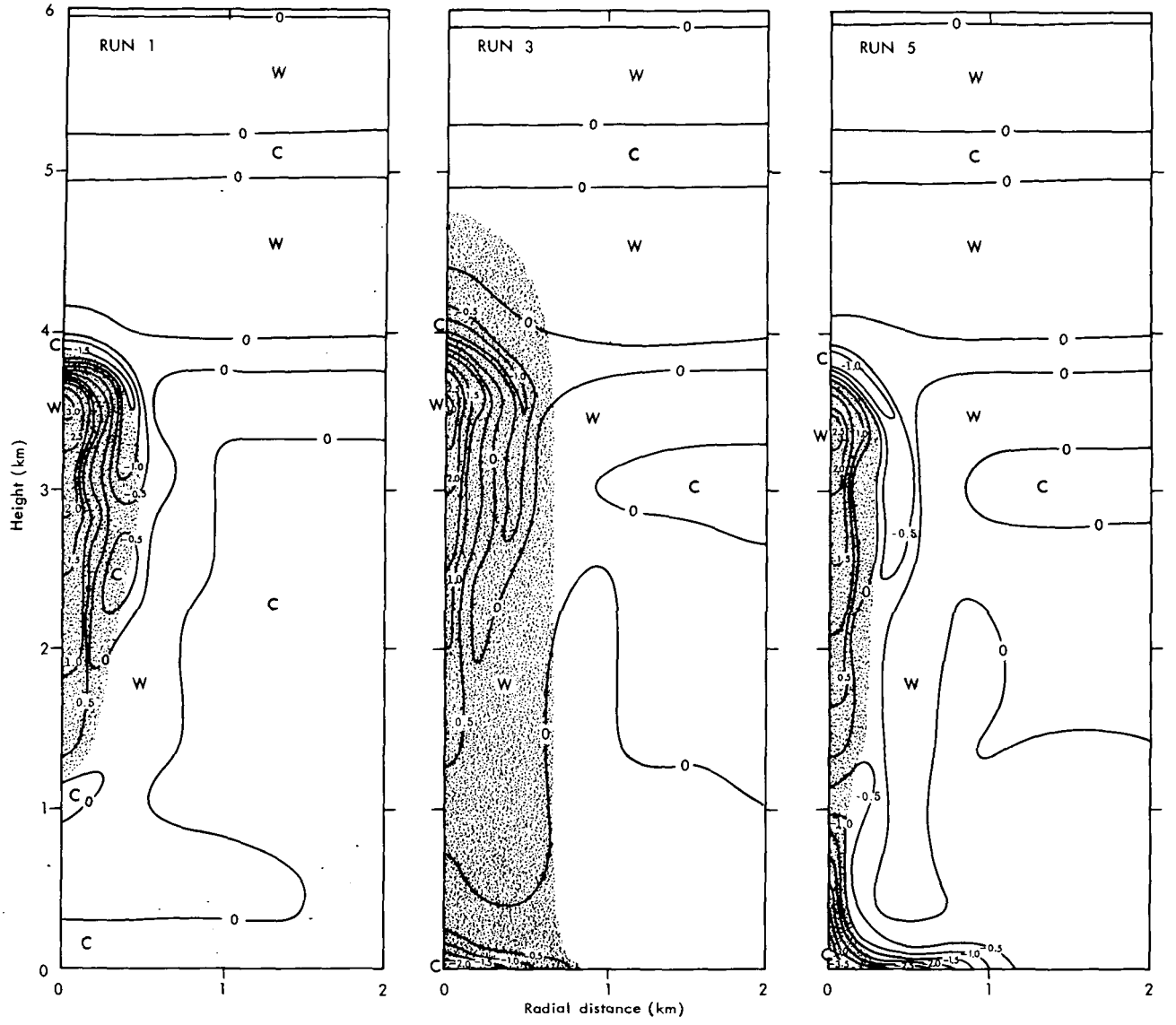

FIGURE 11.—Same as figure 10 for 30 min.

conversion in run 4, but the rate still would have been considerably slower than in run 3. In principle, many different combinations of values of the Berry parameters might be used to simulate clouds of various specific air masses.

Reference to table 3 and figures 2–4 shows that most of the results of these three runs are similar, the differences among them being much less than the differences between them and any of the other three runs. The differences that exist are easily related to the differences in autoconversion and the consequent effect on evaporation rate. Even though autoconversion commenced immediately in runs 3 and 4, it was still of negligible amount at 10 min, when it commenced in run 2. Thereafter, the precipitating water increased more rapidly with Berry maritime autoconversion than with Kessler autoconversion, eventually reaching a higher maximum. With Berry continental autoconversion, precipitating water started its increase considerably later than the other two and never became as great. Because of the slow conversion, run 4 developed more suspended water than the other two, but less total airborne water. Because the rates of condensation were almost identical, this difference must be due to the greater evaporation of run 4 associated with the larger amount of suspended water.

In comparing the Berry maritime and continental autoconversions in a one-dimensional model, Simpson and Wiggert (1969) found that the former grew a slightly taller cloud than the latter, with the difference being ascribed to a larger liquid water content (by 1 $g \cdot m^{-3}$) near the summit of the continental cloud. Our results show the same difference in height, but no such difference in liquid water content. In fact, the continental cloud in our test runs had somewhat less liquid water content throughout than the maritime cloud. We must ascribe the difference to the larger ratio of suspended water to precipitating water in the continental model and its concomitant rate of evaporation. Evaporation resulting

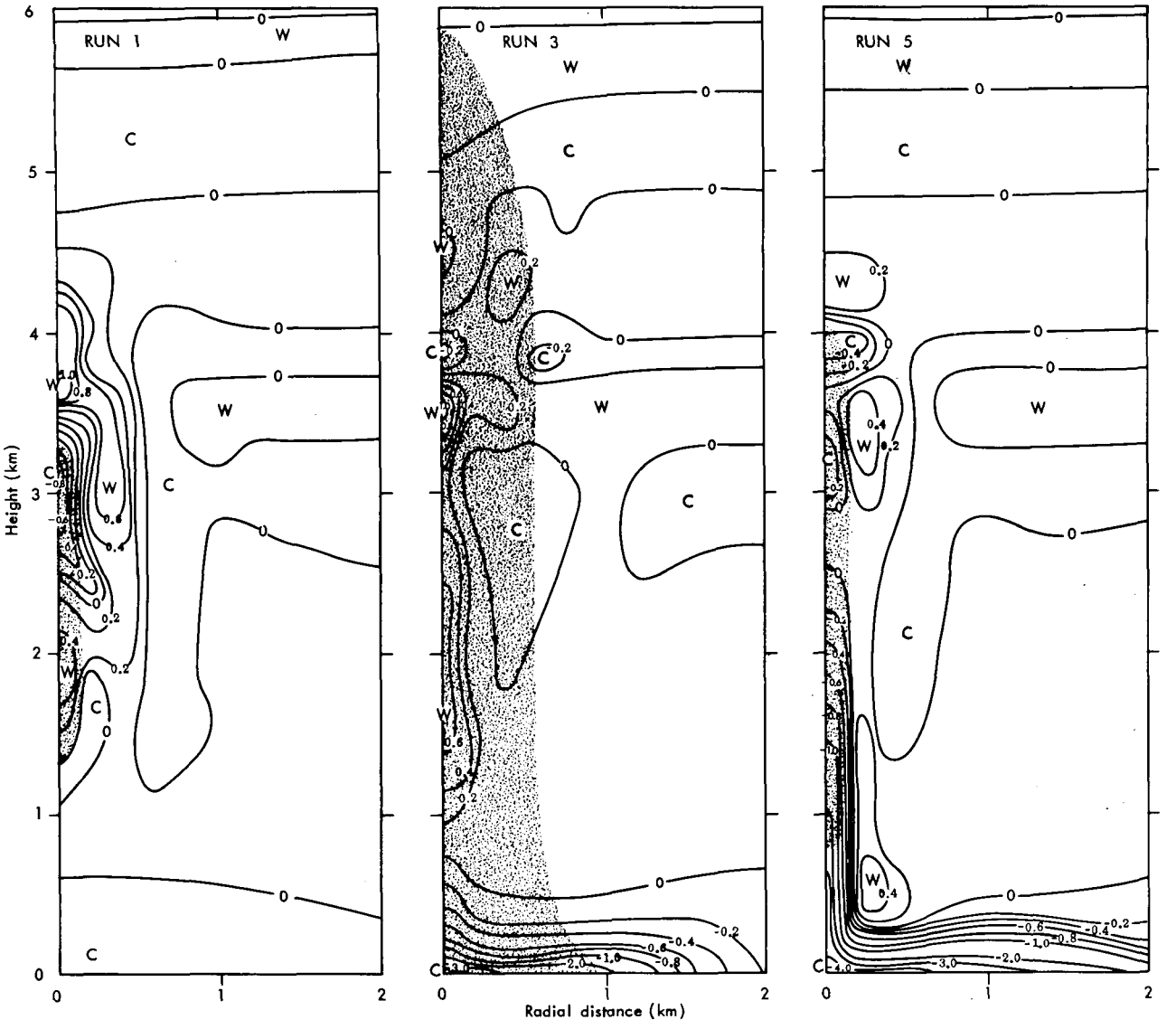

FIGURE 12.—Same as figure 10 for 40 min.

from entrainment is instantaneous in one-dimensional models (similar to the present run 5). Simpson and Wiggert found that the rainfall from the maritime cloud was nearly eight times that from the continental cloud whereas we found the ratio to be about two to one. These figures are not really comparable, however, for the Lagrangian one-dimensional model can calculate only the precipitation falling out of the tower. The two-dimensional model, by contrast, considers precipitation falling from all parts of the cloud and follows it all the way to the earth's surface, taking evaporation into account.

Eddy Diffusion

The treatment of subgrid-scale motions in models of this type is always troublesome. We have not gone into this subject in the present study but have merely included enough Fickian diffusion to assure computational stability. However, after the study was completed, Cotton (1972) pointed out to us that in computing the Laplacians for eq (8)–(11) in cylindrical coordinates we had omitted one term in the case of $r=0$. To test the consequences of this omission, we made another run identical to run 3, but with the additional term.

The inclusion of the missing term, as was expected, reduced the horizontal gradients of the several variables on the central axis and consequently reduced the buoyancy, with the result that the maximum height achieved by the cloudtop decreased from 5800 to 4600 m, still well above the height achieved in run 1 (without the correction). It may be that this result indicates that the eddy coefficient of 40 m^2/s used in the present study is too large.

Other results were affected accordingly but none so drastically as the maximum cloudtop height. For instance, the maximum updraft was reduced only from 15.07 to 11.83 m/s. Interestingly enough, the timing of the various

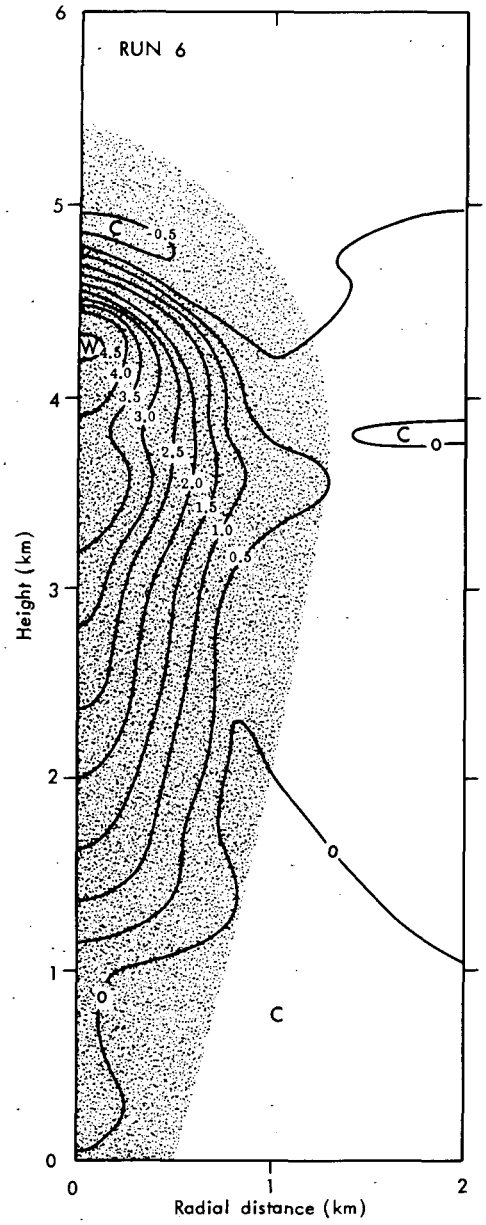

FIGURE 13.—Spatial distribution of departure of virtual temperature (°C) from its initial value for run 6 at 20 min. Area with more than 0.001 g/kg airborne liquid is shaded.

events was hardly affected at all except that the cloud dissipated a few minutes earlier.

On the whole, addition of the missing term improves the results, and it will be included in all future versions of the model. All of its effects are those to be expected from a slight decrease in buoyancy in the most active part of the cloud, and they do not alter in any way our conclusions about the physical processes occurring in and about the cloud.

6. SUMMARY AND CONCLUSIONS

The two-dimensional, numerical cloud model without precipitation gives results in many respects realistic, but the addition of a precipitation mechanism, even through a highly simplified parameterization, produces significant improvement in almost all aspects of the simulation. Specifically, the precipitating model produces higher cloudtops, greater liquid water content, and a smaller summit temperature deficit than the nonprecipitating model. Its maximum updraft is a little weaker, but the downdraft in the subcloud layer is much stronger. In shape, the precipitating cloud has nearly uniform width with height whereas the nonprecipitating cloud tends to develop a less realistic mushroom shape.

The present experiments suggest that most of the differences between the results of the several versions can ultimately be laid to evaporation. Certainly, in those characteristics in which runs 1 and 5 resemble each other but differ from the other runs, evaporation must be the dominant factor. Chief among these characteristics is cloud height. Rapid evaporation about the summit and periphery of the cloud (generally associated with strong entrainment) produces a large temperature deficit, and the cold cap of relatively dense air inhibits continued cloud growth. The model with no evaporative cooling at the summit, on the other hand, developed a negligible cold cap and grew unreasonably large.

The damping effect of the cold cap in the five runs with evaporative cooling appears to be almost independent of the strength or location of the updraft. The maximum updraft occurred at about the same time and altitude in all five of the runs and was strongest in one of the fast-evaporating runs and weakest in the other. Time sections of vertical wind speed indicate that the differences in the actual maxima were smaller than is suggested by the grid-point values shown in table 3. Such differences as occur may well be connected with evaporation in the lower part of the cloud and, in the case of the precipitating cloud, evaporation below cloudbase. The six runs had marked differences in the subcloud downdraft. The nonprecipitating cloud had a negligible downdraft, the cloud with no evaporative cooling had a weak downdraft, the clouds with normal evaporation of precipitation had moderate downdrafts, and the cloud with rapid evaporation of precipitation had a very strong downdraft. These circumstances, together with the computed liquid water contents, strongly suggest that the major factor in developing the downdraft is not water loading but evaporative cooling. This finding is in full agreement with calculations from observations made by Malkus (1955).

It is of particular interest to determine the mechanisms whereby the cloud stops growing and then decays. With the sounding used in the present experiment, the simple parcel method would require a parcel displaced at the condensation level to rise to the tropopause. Typical one-dimensional models modify this by allowing the initial parcel to become progressively diluted with environment air, and, thus, to come to rest at some moderate altitude. Such models can match the altitudes of observed clouds with impressive accuracy. The two-dimensional model is more complex in its interactions, and a full explanation of

the life cycle of its simulated clouds is still not developed. However, enough information is available from these experiments to suggest an explanation of what goes on in the simulated cloud and, it is hoped, in real clouds as well.

In this essentially Eulerian solution of the equations, no physical parcel keeps its identity from one time step to the next, and it is not strictly proper to speak of the cloud as an entity. Any gridpoint with more than 0.001 g/kg of liquid water is arbitrarily considered to be within the cloud, but no specific boundary surface is defined. Nevertheless, such a surface presumably exists between gridpoints, and it is not unrealistic to speak of the cloud as the volume enclosed by that surface.

When a suitable impulse is given to a parcel in a conditionally unstable atmosphere (in the model), the air rises and condensation releases latent heat, causing acceleration of the vertical motion. In the two-dimensional model, a return flow is set up outside the cloud, and a supply of moist air enters both vertically and horizontally at low levels. As the active core of the cloud rises, a small circulation resembling a spherical vortex appears, and more and more of the air entering the cloud is from higher and drier levels. Moreover, lifting and evaporation at the top produce a cold cap, and the cold, dry air is brought down along the periphery where it mixes with cloudy air to produce further evaporation and cooling. This cap of cold, dense air being dragged into the cloud eventually stops the upward motion of the cloud vortex. The altitude at which this occurs is in part a function of the rate of evaporation; thus, it was high in runs 2–4 and low in runs 1 and 5. In run 6, without effective cold cap, growth was stopped only with the cloud's arrival at the upper limit of the computational space.

Even in the nonprecipitating model, a weak counter cell appears below the cloud, and the downdraft cuts off the supply of moisture through the base. Flow into the cloud then comes from increasingly higher, generally dryer, levels. Eventually the downdraft around the periphery also cuts off the inflow of moist air from the sides, and the cloud erodes laterally, finally vanishing.

In the precipitating models, the rain falling below the original cloudbase evaporates, and a relatively strong circulation cell is established with a downdraft below the cloud. Away from the cloud axis, the downdraft extends to higher levels than it does at the axis, cutting off the inflow to the lower part of the cloud but permitting some inflow at middle levels. The downdraft around the upper periphery connected with the cold cap is, of course, less intense than in the nonprecipitating model. Thus, there is less lateral erosion, and the rain falling below the original cloudbase maintains the original cloud radius because of its slow rate of evaporation. After about 30 min, even in the precipitating models, all inflow is effectively cut off, and thereafter the cloud decays. If there is no evaporative cooling, however, the cloud does not erode. In fact, as the cloud approaches the ceiling, it grows in radius. This is probably a consequence of the distortion in flow patterns caused by the rigid boundaries, as is the appearance and subsequent disappearance of a downdraft below the cloud.

A somewhat puzzling result of the present experiment was that in all six runs, regardless of their microphysics, the maximum updraft, which signals the dynamic peak of cloud development, occurred at 30 min. Previous experience (Murray 1971) suggests that this time of maximum is a function of the basic sounding and of the nature of the initial impulse. There may be other influences at work, however, and further study of this feature is indicated.

The principal deficiency of the model as it now stands is its failure to treat the ice phase. Work is now in progress to incorporate a parameterization of processes involving ice crystals. This should make the model not only more realistic, but more useful for studying cloud modification.

ACKNOWLEDGMENTS

The work reported here was supported under Contract DAHC15 67 C 0141 with the Defense Advanced Research Projects Agency. The authors wish to express special appreciation to Joanne Simpson for her critical reading of this paper and for se eral helpful suggestions.

REFERENCES

'Arnason, Geirmundur, Brown, Philip S., and Chu, Roland T., "Numerical Simulation of the Macrophysical and Microphysical Processes of Moist Convection," *Proceedings of the WMO/IUGG Symposium on Numerical Weather Prediction, Tokyo, Japan, November 26–December 4, 1968*, Japan Meteorological Agency, Tokyo, Mar. **1969**, pp. I–11—I–21.

'Arnason, Geirmundur, Greenfield, R. S., and Newburg, E. A., "A Numerical Experiment in Dry and Moist Convection Including the Rain Stage," *Journal of the Atmospheric Sciences*, Vol. 25, No. 3, May **1968**, pp. 404–415.

Berry, Edwin X., "Modification of the Warm Rain Process," *Proceedings of the First National Conference on Weather Modification, Albany, New York, April 28–May 1, 1968*, American Meteorological Society, Boston, Mass., **1968**, pp. 81–85.

Cotton, William, Experimental Meteorology Laboratory, NOAA, Miami, Fla., Feb. 24, **1972** (personal communication).

Gunn, Ross, and Kinzer, Gilbert D., "The Terminal Velocity of Fall for Water Droplets in Stagnant Air," *Journal of Meteorology*, Vol. 6, No. 4, Aug. **1949**, pp. 243–248.

Kessler, Edwin, III, "On the Continuity of Water Substance," *ESSA Technical Memorandum* IERTM–NSSL 33, U.S. Department of Commerce, National Severe Storms Laboratory, Norman, Okla., Apr. **1967**, 125 pp.

Kessler, Edwin, III, "On the Distribution and Continuity of Water Substance in Atmospheric Circulations," *Meteorological Monographs*, Vol. 10, No. 32, American Meteorological Society, Boston, Mass., Nov. **1969**, 84 pp.

Koenig, L. Randall, "Numerical Test of the Validity of the Drop-Freezing/Splintering Hypothesis of Cloud Glaciation," *Journal of the Atmospheric Sciences*, Vol. 23, No. 6, Nov. **1966**, pp. 726–740.

Liu, Y. Y., and Orville, Harold D., "Numerical Modeling of Precipitation and Cloud Shadow Effects on Mountain-Induced Cumuli," *Journal of the Atmospheric Sciences*, Vol. 26, No. 6, Nov. **1969**, pp. 1283–1298.

Malkus, Joanne S., "Some Results of a Trade-Cumulus Cloud Investigation," *Journal of Meteorology*, Vol. 11, No. 3, June **1954**, pp. 220–237.

Malkus, Joanne S., "On the Formation and Structure of Downdrafts in Cumulus Clouds," *Journal of Meteorology*, Vol. 12, No. 4, Aug. **1955**, pp. 350–354.

Malkus, Joanne S., and Witt, G., "The Evolution of a Convective Element: A Numerical Calculation," *The Atomsphere and the Sea in Motion*, Rockefeller Institute Press, New York, N.Y., **1959**, pp. 425–439.

Marshall, J. S., and Palmer, W. McK., "The Distribution of Raindrops With Size," *Journal of Meteorology*, Vol. 5, No. 4, Aug. **1948**, pp. 165–166.

Murray, Francis W., "Numerical Models of a Tropical Cumulus Cloud With Bilateral and Axial Symmetry," *Monthly Weather Review*, Vol. 98, No. 1, Jan. **1970**, pp. 14–28.

Murray, Francis W., "Humidity Augmentation as the Initial Impulse in a Numerical Cloud Model," *Monthly Weather Review*, Vol. 99, No. 1, Jan. **1971**, pp. 37–48.

Ogura, Yoshimitsu, "Convection of Isolated Masses of a Buoyant Fluid: A Numerical Calculation," *Journal of the Atmospheric Sciences*, Vol. 19, No. 6, Nov. **1962**, pp. 492–502.

Ogura, Yoshimitsu, "The Evolution of a Moist Convective Element in a Shallow, Conditionally Unstable Atmosphere: A Numerical Calculation," *Journal of the Atmospheric Sciences*, Vol. 20, No. 5, Sept. **1963**, pp. 407–424.

Orville, Harold D., and Sloan, Lansing J., "A Numerical Simulation of the Life History of a Rainstorm," *Journal of the Atmospheric Sciences*, Vol. 27, No. 8, Nov. **1970**, pp. 1148–1159.

Simpson, Joanne, Simpson, R. H., Andrews, D. A., and Eaton, M. A., "Experimental Cumulus Dynamics," *Reviews of Geophysics*, Vol. 3, No. 3, Aug. **1965**, pp. 387–431.

Simpson, Joanne, and Wiggert, Victor, "Models of Precipitating Cumulus Towers," *Monthly Weather Review*, Vol. 97, No. 7, July **1969**, pp. 471–489.

Simpson, Joanne, and Wiggert, Victor, "1968 Florida Cumulus Seeding Experiment: Numerical Model Results," *Monthly Weather Review*, Vol. 99, No. 2, Feb. **1971**, pp. 87–118.

Srivastava, R. C., "A Study of the Effect of Precipitation on Cumulus Dynamics," *Journal of the Atmospheric Sciences*, Vol. 24, No. 1, Jan. **1967**, pp. 36–45.

Weinstein, Alan I., "A Numerical Model of Cumulus Dynamics and Microphysics," *Journal of the Atmospheric Sciences*, Vol. 27, No. 2, Mar. **1970**, pp. 246–255.

Wexler, Raymond, and Malkus, Joanne S., "Observations of Tropical Clouds: Results of the 1956 Caribbean Aircraft Expedition," *Report* No. 58–46, Woods Hole Oceanographic Institution, Mass., **1958**, 122 pp.

Wobus, Hermann B., Murray, Francis W., and Koenig, L. Randall, "Calculation of the Terminal Velocity of Water Drops," *Journal of Applied Meteorology*, Vol. 10, No. 4, Aug. **1971**, pp. 751–754.

[*Received December 17, 1971; revised April 13, 1972*]